ChemSusChem

Asymmetric supercapacitors based on rGO-PMo12 as a positive and rGO-PW12 as a negative electrode

--Manuscript Draft--

Manuscript Number:	
Article Type:	Communication
Corresponding Author:	Deepak Dubal, Ph.D. Spain Barcelona, SPAIN
Corresponding Author E-Mail:	dubaldeepak2@gmail.com
Order of Authors (with Contributor Roles):	Deepak Dubal, Ph.D.
	Nilesh Chodankar
Keywords:	Asymmetric supercapacitor, Nanocarbon, reduced graphene oxide, polyoxometalates, Nanohybrid
Manuscript Classifications:	Electrode materials; Energy storage materials; Graphene; Hybrid materials; Supercapacitors
Suggested Reviewers:	Keryn Lian keryn.lian@utoronto.ca
	Yupin Wu wuyp@fudan.edu.cn
	D. R. Patil deepphy24@gmail.com
	Dongfang Yang Dongfang.Yang@nrc-cnrc.gc.ca
Opposed Reviewers:	
Abstract:	Nanofabrication via "bottom-up" approach of hybrid electrode materials into well-defined architecture is essential for the next generation miniaturized energy storage devices. This paper describes the design and fabrication of reduced graphene oxide (rGO)/polyoxometalates (POMs) based hybrid electrode materials and their successful exploitation for asymmetric supercapacitor. Firstly, the redox active nanoclusters of POMs (phosphomolybdic acid (PMo12) and phosphotungstic acid (PW12)) are uniformly decorated on the surface of rGO nanosheets to take full advantage of both charge-storing mechanisms (faradaic from POMs and electric double layer from rGO). The as-synthesized rGO-PMo12 and rGO-PW12 hybrid electrodes exhibits great electrochemical performances with specific capacitance of 299 F/g (269 mF/cm2) and 370 F/g (369 mF/cm2) in 1 M H2SO4 electrolyte at 5 mA/cm2, respectively. Later, asymmetric supercapacitors was fabricated using rGO-PMo12 as a positive and rGO-PW12 as negative electrodes. This novel rGO-PMo12//rGO-PW12 asymmetric cell could be successfully cycled in a wide voltage window up to 1.6 V and hence exhibits excellent energy density of 39 Wh/kg (1.3 mWh/cm3) at a power density of 658 W/kg (23 mW/cm3).
Author Comments:	To, The Editor, ChemSusChem Dear Editor, This submission implies online submission of our recent novel investigation entitled "Asymmetric supercapacitors based on rGO-PMo12 as a positive and rGO-PW12 as a negative electrode" Deepak P. Dubal,a* Nilesh R. Chodankar,b for publication in ChemSusChem Polyoxometalates (POMs) are clusters of anionic molecular metal oxide which includes variety of transition metals such as Mo, W, V etc. Within the field of energy storage,

	POMs have found a particularly well-suited niche application in supercapacitors, initially integrated in conducting polymers and more recently forming hybrid electrodes with carbon materials. POMs can exhibits high energy density for supercapacitors due to the rapid and reversible multi-electron redox reactions. On the other hand, an emerging concept of fabricating asymmetric SCs stimulate the energy storing capacity by extending the operating voltage boundary of the device (E=0.5CV2). Thus, taking advantages of both these characteristics we expected to assemble a high energy density supercapacitor. Only one report is available on the asymmetric configuration using polyoxometalates based nanocomposite. Authors have prepared Polypyrrole/Phosphomolybdic Acid//Poly(3,4-ethylenedioxythiophene)/Phosphotungstic Acid Asymmetric Supercapacitor. (J. Electrochem. Soc., 2010, 157, A1030-A1034) with only small improvement in the electrochemical properties of device. In present investigation, initially we have prepared two different nanohybrids based on reduced graphene oxide (rGO)/polyoxometalates (in this case rGO-PMo12 and rGO-PW12) in order to take full advantage of both charge-storing mechanisms (faradaic from POMs and electric double layer from rGO). The as-synthesized rGO-PMo12 and rGO-PW12 hybrid electrodes were further tested in conventional three electrode system and realised acceptable specific capacitance but in different operating potentials. Thus, taking this advantage of these nanohybrids, asymmetric supercapacitors was fabricated with rGO-PMo12 as a positive and rGO-PW12 as negative electrodes. Impressively, this rGO-PMo12//rGO-PW12 asymmetric cell can be successfully cycled in a wide voltage range up to 1.6 V which results in excellent energy density of 39 Wh/kg (1.3 mWh/cm3) at a power density of 658 W/kg (23 mW/cm3). These values are significantly higher than the previously reported values, suggesting the potential of this new hybrid device based on hybrid electrodes for many promising energy storage applications I really hope you will agree that this excellent report could be a promising article for many interesting reports to come. I look forward to your news Best Regards Dr. Deepak P. Dubal, Ph. D. Vice Chancellor's Fellow Former Marie-Curie (BP-DGR) and Humboldt Fellow School of Chemical Engineering, The University of Adelaide, Adelaide, South Australia 5005, Australia
Section/Category:	
Additional Information:	
Question	**Response**
Dedication	NO
Submitted solely to this journal?	Yes
Has there been a previous version?	No
Do you or any of your co-authors have a conflict of interest to declare?	No. The authors declare no conflict of interest.

Asymmetric supercapacitors based on rGO-PMo_{12} as a positive and rGO-PW_{12} as a negative electrode

Deepak P. Dubal,[a, b]* Nilesh R. Chodankar* [c]

[a] School of Chemical Engineering, The University of Adelaide, Adelaide, South Australia 5005, Australia

[b] Catalan Institute of Nanoscience and Nanotechnology (ICN2), The Barcelona Institute of Science and Technology (CSIC-BIST), Campus UAB, Bellaterra, 08193 Barcelona, Spain

[c] School of Applied Chemical Engineering, Chonnam National University, Gwangju 500-757, South Korea

CORRESPONDING AUTHOR FOOTNOTE

Dr. Deepak Dubal

Tel.: +61-8-3131535 Fax: +61-8-83134373

E-mail: dubaldeepak2@gmail.com (D. Dubal),

Abstract

Nanofabrication via "bottom-up" approach of hybrid electrode materials into well-defined architecture is essential for the next generation miniaturized energy storage devices. This paper describes the design and fabrication of reduced graphene oxide (rGO)/polyoxometalates (POMs) based hybrid electrode materials and their successful exploitation for asymmetric supercapacitor. Firstly, the redox active nanoclusters of POMs (phosphomolybdic acid (PMo_{12}) and phosphotungstic acid (PW_{12})) are uniformly decorated on the surface of rGO nanosheets to take full advantage of both charge-storing mechanisms (faradaic from POMs and electric double layer from rGO). The as-synthesized rGO-PMo_{12} and rGO-PW_{12} hybrid electrodes exhibits great electrochemical performances with specific capacitance of 299 F/g (269 mF/cm^2) and 370 F/g (369 mF/cm^2) in 1 M H_2SO_4 electrolyte at 5 mA/cm^2, respectively. Later, asymmetric supercapacitors was fabricated using rGO-PMo_{12} as a positive and rGO-PW_{12} as negative electrodes. This novel rGO-PMo_{12}//rGO-PW_{12} asymmetric cell could be successfully cycled in a wide voltage window up to 1.6 V and hence exhibits excellent energy density of 39 Wh/kg (1.3 mWh/cm^3) at a power density of 658 W/kg (23 mW/cm^3).

Keywords: Asymmetric supercapacitor, Nanocarbon, reduced graphene oxide, polyoxometalates, Nanohybrid

Introduction

The dominating applications of recent electronic devices such as portable devices (mobiles, laptops etc.) as well as a storage of renewable energies (solar, wind etc.) requires efficient energy storage devices [1, 2]. The most promising and convenient systems for energy storage are batteries and supercapacitors (SCs) where the former stores the energy through bulk redox reactions while in later charges are stored through either electrostatic (electric double layer capacitance) or surface redox reactions (pseudocapacitor) [3, 4]. Among which SCs are the promising once due to their delightful cycle stability, fast charge/discharge rate and, safe and reliable operation [6]. However, the narrow energy storing capability of existing SCs upsetting their practical application [7]. In this context, an emerging concept of fabricating asymmetric SCs stimulate the energy storing capacity by extending the operating voltage boundary of the device ($E=0.5CV^2$) [1]. However, different charge storing mechanisms of both electrodes in asymmetric cell limits their electrochemical performances. Therefore, it is very crucial to investigate the electrode materials which can provide high electrochemical performance in terms of wide operating voltage, high specific capacitance and extended cycling stability.

The most intuitive approach to get higher energy density as well as power density for SCs is to fabricate the asymmetric (hybrid) device with hybrid electrodes that helps to improve capacitance as well as operating voltage (since $E=0.5\ CV^2$). The hybrid electrodes combines the features of EDLC and pseudocapacitance (faradic) in a single electrode [8-10] which consequently improves the capacitance.

Recently, the hybrid materials based on redox active polyoxometalates (POMs) with carbon-based materials have shown a great potential for high performance SCs application [11-15]. Basically, POMs are the polyatomic ion, usually consists an anion of the early transition metals (such as V, Mo, W Ta, Nb etc.) linked with oxygen to form a three dimensional cluster

[16, 17]. These nanometric molecular clusters are very stable and have a stable interaction with various electrode materials like graphene, different conducting polymers [18-20]. One of the most noteworthy properties of POMs is the ability of accept and release an electrons without changing their structural features that makes it suitable electrodes for SCs. In addition, anchoring these redox capable POMs nanometric molecular clusters on carbon materials, effectively increase electroactive sites for electrochemical reactions and therefore resultant electrochemical performance will be increased.

In present work, we have developed the novel asymmetric SCs device using the POMs and graphene based hybrid electrodes. Primarily, the open-porous three-dimensional (3D) reduced graphene oxide (rGO) was prepared using modified Hummers method. In order to prepare hybrid electrodes, the surface of rGO nanosheets were uniformly anchored with nanoclusters of phosphomolybdic acid (PMo_{12}) and phosphotungstic acid (PW_{12}). As it will be shown, these materials present a synergic combination with a dual charge storage mechanism: electrical double layer (EDL, nanocarbons) and redox (faradaic, PMo_{12} or PW_{12}). The electrochemical features of hybrid electrodes rGO-PMo_{12} and rGO-PW_{12} were investigated in 1 M H_2SO_4 electrolyte with conventional three electrode configuration. In the next step, asymmetric cell was assembled with rGO-PMo_{12} (positive electrode) and rGO-PW_{12} (positive electrode) in 1 M H_2SO_4 electrolyte. All the electrochemical properties were systematically investigated.

Experimental

Preparation of rGO, rGO–PMo_{12} and rGO-PW_{12} hybrids electrodes

Primarily, the graphene oxide (GO) was prepared by the modified Hummers method in which natural graphite powder used as a source. In order to prepare reduced graphene oxide (rGO) thermal treatment process was used. The suitable amount of GO was heated for 1 h at

temperature 800°C under the flow of nitrogen. Later, the hybrid materials rGO-PMo_{12} and rGO-PW_{12} were prepared according to our previous report [21, 22]. Firstly, 0.5 g of rGO was dispersed in 200 ml of deionized water (DI) for 30 min with a probe sonicator. In which 10 mM of phosphomolybdic acid or phosphotungstic acid was added into two separately sonicated 100 ml rGO dispersion. Note that the concentrations of PMo12 and PW12 are already optimized in our previous study in order to get uniform coating on rGO without aggregation. Furthermore, these solutions were bath sonicated for 2 h and kept at room temperature for 24 h. Finally, the products were filtered, washed with DI water and dried in a vacuum oven at 80 °C over night.

Electrochemical measurements

To measure the electrochemical properties of prepared hybrid material, electrode preparation is very essential. The electrodes were fabricated on the piece of flexible carbon cloth by casting a paste composed of active material (rGO-PMo_{12} or rGO-PW_{12}), acetylene black and polyvinylidene fluoride (PVDF) in the ratio of 85%:5%:10% with few drops of N-methyl-2-pyrrolidone (NMP). The cyclic voltammetry (CV) and galvanostatic charge–discharge (CD) measurements were carried out using the Biologic VMP3 potentiostat. The asymmetric SC was assembled using Swagelok® cells where rGO-PMo_{12} and rGO-PW_{12} were taken as positive and negative electrodes, respectively with 0.5 M H_2SO_4 electrolyte socked separator.

Results and discussion

With very simple chemical strategy, two different hybrid materials such as rGO-PMo_{12} and rGO-PW_{12} were prepared. The oxygen functional groups present at the surface of rGO will acts as anchoring centers for the decoration of POMs (PMo_{12} and PW_{12}). The effective anchoring of POMs nanoclusters on rGO nanosheets were inspected by different surface morphological techniques and shown in Figure 1. The rGO is composed of the ultrathin nanosheets which allows the large active sites for holding the nanoclusters of POMs as seen in

the Fig. 1 (a, b). More importantly, the interspace in between two neighboring nanosheets allows the special “high-way” for the electron transport by maintaining the good ionic conductivity. It is interesting to note that, the open porous morphology of rGO nanosheets remains unaltered even after the heavy anchoring of POM nanoclusters (see S. I. S1). The rGO surface is uniformly decorated with tiny nanoclusters of the POMs as confirmed from STEM images (Fig. 1(c, d)). These tiny PMo_{12} and PW_{12} nanoclusters attached to the rGO nanosheets not only prevents the re-stacking of graphene but also forms mesopores which can provides easy paths for ion diffusion and electron transport. The TEM-EDAX of the rGO-PMo_{12} and rGO-PW_{12} hybrid samples is shown in Fig. 1 (e, f) which clearly confirms the effective anchoring of POMs on the rGO nanosheets as it shows the stronger peaks for Mo and W.

The broad XPS spectra for rGO-PMo_{12} and rGO-PW_{12} hybrid are shown in Fig. 2 (a) which undoubtedly specify the presence of carbon, oxygen and desired elements (Mo and W). Fig. 2 (b) presents the narrow scan spectrum for the C1s which is fitted by three peaks at 288.5 eV, 284.4 and 285.2 binding energies confirming the formation of reduced graphene oxide (rGO). Further, the core-level XPS spectrum of Mo3d for rGO-PMo_{12} shows two pairs of Gaussian peaks at the binding energies of 235.7 and 232.6 eV (see Fig. 2(c)). These peaks correspond to $3d_{3/2}$ and $3d_{5/2}$ suggesting that molybdenum is in (VI) oxidation state [23, 24]. Similarly, for the rGO-PW_{12} sample, the narrow scan spectrum for W4f is fragmented into two prominent peaks centered at the binding energies of 37.8 and 35.7 eV (Fig. 2(d)) which are assigned for the $4f_{5/2}$ and $4f_{7/2}$ levels of tungsten in the (VI) oxidation state [25]. BET analyses of rGO, rGO-PMo_{12} and rGO-PW_{12} showed that all the samples exhibit high surface areas of 242.4 m^2/g, 231.2 m^2/g and 237.3 m^2/g (see S.I. S2). The slight decrease in the active surface for rGO-POMs sample is attributed to the inclusion of the POM nanoparticles, which contribute heavily to the total mass of the hybrid.

To evaluate the operating potential range of the prepared hybrid electrodes for SCs application, firstly it is necessary to carry out the electrochemical measurements in standard three-electrode arrangement. Fig. 3 (a, b) shows the cyclic voltammetry curves for the rGO-PMo_{12} and rGO-PW_{12} hybrid electrodes at different scan rates in 1 M H_2SO_4 electrolyte, respectively. The CV curves for both the hybrid electrodes exhibit nearly rectangular nature with obvious redox waves, confirming the dual charge storing mechanism such as EDLC (nanocarbon rGO) and redox reactions (PMo_{12} and PW_{12}). All the metal moieties such as Mo and W in PMo_{12} and PW_{12} are at the surface of nanoclusters, hence can be easily accessed by the electrolyte ions, and thus undergoes the fast reversible multi-electron redox processes similar to the quantum sized oxide particles. Further, it is interesting to note that, the shapes of the CV profiles does not change at higher scan rate for both the hybrids, suggesting that the rGO nanosheets actually facilitates fast electronic and ionic transport and thus improves the rate capability of the electrodes. The galvanostatic charge-discharge measurements are carried out at different current densities for both the hybrid electrodes (Fig. 3 (c, d)). The shapes of the charge-discharge curves are considerably different from the ideal triangular shape, which strongly suggest the involvement of both charge-storing mechanisms similar to the CV results. Further, to calculate the rate capability of the prepared electrode, the specific and areal capacitance is calculated for various current densities and plotted in Fig. 3 (e, f). The rGO-PMo_{12} and rGO-PW_{12} hybrid electrodes shows the highest specific capacitance of 299 and 370 F/g for the mass loading of 1 mg/cm^2 (269 and 370 mF/cm^2) at lower current density of 5 mA/cm^2, respectively. Amazingly, even at higher current density of 30 mA/cm^2 both the hybrid electrode shows excellent capacity retention by maintaining about 52 and 65% initial capacitance for rGO-PMo_{12} and rGO-PW_{12}, respectively.

The detailed charge storing kinetics can be revealed by the relation of current (i) and scan rate in CV curves which is described by the following equation:

$$i = a\nu^{b} \quad (1)$$

where i is the peak current (mA), ν is the scan rate (mV/s), a and b are coefficients. The value of b defines the type of charge-storing mechanism whether it is capacitive or diffusion-controlled. While b = 0.5 suggest the semi-infinite diffusion-controlled process and b = 1 suggests the contribution from capacitive behaviour. The values of 'b' can be calculated by fitting a plot of log(anodic current) vs log(scan rate) as shown in Figure 4 (a) which are found to be 0.84 and 0.72 for rGO-PMo_{12} and rGO-PW_{12} hybrids respectively. This further confirms that surface-controlled capacitive electrode process dominates the rGO-PMo_{12} and rGO-PW_{12} hybrids electrodes [26]. Thus, the total voltammetric charge (q) stored in the electrode is a contribution from surface capacitive (Q_c) and the diffusion-controlled charges (Q_d) which can be expressed as follow;

$$Q_t = Q_c + k\nu^{-1/2} \quad (2)$$

where, k is the constant and ν is the scanning rate. Fig. 4 (b) is the plot of the Q_t against the reciprocal of the square root of the scan rate for for rGO-PMo_{12} and rGO-PW_{12} hybrids. The deviation in the linearity at high scan rate is due to the polarization effect which is ignored from the above equation. The extrapolation of the linear fit to the data to the y-intercept give the values of surface capacitive contribution (Q_c). The plot of the capacitive (Q_c) and diffusion-controlled (Q_d) contributions to the total stored charges at various scan rates is shown in Fig. 4 (c). Interestingly, at low scan rate (5 mV/s), the surface contributes around 62% and 59% of the total capacity for rGO-PMo_{12} and rGO-PW_{12} electrodes, respectively. These results suggest that the rGO-PMo_{12} and rGO-PW_{12} electrodes are mainly pseudo-capacitive (surface redox) in nature during the charge/discharge process.

Fig. 5 shows the schematic illustration of asymmetric cell design based on rGO-PMo_{12} and rGO-PW_{12} electrodes. It is seen that rGO-PMo_{12} electrode works within the potentials of -0.2 V to 1.0 V (vs, Ag/AgCl) while the rGO-PW_{12} shows the good CV trace within the potential range

of -0.6 V to 1.0 V (vs, Ag/AgCl). Thus, it is interesting that, the adsorption of PW_{12} on the surface of rGO nanosheets not only add extra redox-active species but also provides overpotentials (S. I. S4). These unique electrochemical features of rGO-PMo_{12} and rGO-PW_{12} hybrid electrodes motivate us to pair them together in asymmetric cell which is expected to offer high capacitance (due to dual charge storing in hybrids) with extended working voltage, consequently high energy density. In this context, asymmetric SC is fabricated using the rGO-PMo_{12} (positive electrode) rGO-PW_{12} (negative electrode) in 1 M H_2SO_4 electrolyte. Note that, the charges stored in both electrodes need to be balanced in order to take advantage of full voltage window which can be done by balancing mass of the material [26]. Thus, the estimated mass ratio is 1.7:1 for rGO-PMo_{12}:rGO-PW_{12} which results the total mass loading of 3.1 mg (in both electrodes). The CV curves for rGO-PMo_{12}//rGO-PW_{12} asymmetric cell at different scan rates within voltage range of 1.6 V are presented in Fig. 6 (a). The CV curves exhibit box-shapes with redox waves further confirming the effective utilization of the anchored redox-active species (PMo_{12} and PW_{12}). In addition, the profile of CV curves is maintained even at high scan rates suggesting excellent capacitive features of the rGO-PMo_{12}//rGO-PW_{12} asymmetric cell. The representative charge-discharge curve for rGO-PMo_{12}//rGO-PW_{12} cell at a constant current density of 15 mA/cm^2 with corresponding potential distribution across positive and negative electrodes is shown in Fig. 6 (b). It is noted that the positive and negative electrode contributes equal potentials for the full asymmetric cell. The positive electrode contribute the operating potential from +0.4 to +1.2 V (Vs Ag/AgCl), while negative electrode works within +0.4 to -0.4 V (Vs, Ag/AgCl). Thus, it is confirmed that the anchoring of PW_{12} onto rGO offers overpotential and can effectively works as negative electrode in asymmetric cell as we expected (S. I. S5). Furthermore, the charge-discharge curves for rGO-PMo_{12}//rGO-PW_{12} cell were measured at various current densities (see Fig. 6 (c)). The CD curves are non-triangular in shape due to the redox-active species and can be easily cycled in a wide voltage window of 1.6 V. To investigate

the rate capability of rGO-PMo_{12}//rGO-PW_{12} device, the specific and volumetric capacitance is estimated from charge/discharge curves and plotted in Fig. 6 (d). The asymmetric cell exhibits the maximum gravimetric capacitance of 110.9 F/g (3.91 F/cm^3, calculated by measuring the volume of device, V= 0.0689 cm^3) at lower current density of 2 mA/cm^2. Moreover, even at high current density of 20 mA/cm^2, asymmetric cell maintains 40 % of its initial capacitance suggesting good rate capability.

The energy and powder densities are the fundamental parameters of the energy storage devices. Therefore, it is necessary to calculate these parameters by considering the charge-discharge curves. Fig. 7 (a) presents the Ragone plot for the rGO-PMo_{12}//rGO-PW_{12} asymmetric cell. The device show the high energy density of 1.39 mWh/cm^3 (39.45 Wh/kg) at power density of 23 mW/cm^3 (658 W/kg). Furthermore, it is interesting to note that even at higher power density of 232 mW/cm^3 (6583 W/kg) the asymmetric cell shows 0.5 mWh/cm^3 (15.63 Wh/kg) energy density, suggesting excellent electrochemical features of the PMo_{12}//rGO-PW_{12} asymmetric SC. These values are considerably higher than the POM based symmetric and asymmetric cells as well as other metal oxide based supercapacitors [12, 13, 21, 22, 28]. For instance, Suppes et al. [28] assembled Polypyrrole/Phosphomolybdic Acid //Poly(3, 4 ethylenedioxythiophene)/Phosphotungstic Acid (PPy/PMo_{12}//PEDOT/PW_{12}) asymmetric cell and reported specific energy of 4 Wh/kg (at specific power of 103 W/kg). The cycling stability is another major issue of energy storage devices. The high cycling stability of the energy storage devices are valuable for controlling the maintenance cost of the electronic devices. The stability of our rGO-PMo_{12}//rGO-PW_{12} asymmetric SCs cell is evaluated by running 2000 charge-discharge cycles at identical current density of 10 mA/cm^2. Fig. 7 (b) represent the plot of capacity retention and Coulombic efficiency with cycle number and the inset of figure shows few CD cycles. The rGO-PMo_{12}//rGO-PW_{12} device displays an excellent cycling stability by holding the 95 % of its initial capacity and a Coulombic efficiency of almost more than 94 % after 2000

cycles. The loss in the initial capacitance after 2000 charge-discharge cycles credited to the surface redox reactions.

The electrochemical performance of the rGO-PMo_{12}//rGO-PW_{12} cell was investigated by EIS measurements. Fig. 8 (a) displays the Nyquist plot for rGO-PMo_{12}//rGO-PW_{12} asymmetric cell which consists of very small equivalent series resistance (ESR) of 0.6 Ω/cm^2, obtained from non-zero intercept on X-axis. The whole credit of excellent electrochemical performance goes to the unique architecture of the electrodes as well as synergic contribution from rGO and POMs. The uniform anchoring of POMs on the rGO nanosheets not only provides faradic contribution but also enhance the electroactive surface area. The inset of Fig. 8 (a) shows the phase angle of rGO-PMo_{12}//rGO-PW_{12} cell which is close to 90° ($\theta \approx 75^{o}$), revealing an ideal capacitor performance [29]. Moreover, the ideal capacitive behavior of the electrode is to estimate the frequency at which the phase angle crosses 45° angle [30]. For example, the commercial activated carbon based EDLCs shows a 45° phase angle at the frequency of ~0.2 Hz [31]. In the present investigation, the rGO-PMo_{12}//rGO-PW_{12} cell show the phase angle of 45° at a frequency of ~5.24 Hz (τ_0 = 0.19 sec), suggesting a rapid frequency response and excellent capacitive behavior. Furthermore, the electrochemical performance of the cell can also be evaluated by calculating the real and imaginary capacitances at a corresponding frequency [32]:

$$C(\omega) = C^{'}(\omega) - jC^{''}(\omega) \quad (3)$$

Where,

$$C^{'}(\omega) = \frac{Z^{''}(\omega)}{\omega \mid Z(\omega) \mid^2} \quad (4)$$

$$C^{''}(\omega) = \frac{Z^{'}(\omega)}{\omega \mid Z(\omega) \mid^2} \quad (5)$$

where '*Z'* the complex impedance represented as $Z(\omega) = Z'(\omega) + Z''(\omega)$ and $\omega = 2\pi f$ where *f* is the frequency. $C'(\omega)$ is the real accessible capacitance of the electrode while $C''(\omega)$ is the energy loss due to the irreversible processes of the electrodes, Z' and Z'' are the real and imaginary parts of the Nyquist plot, respectively. Further, Fig. 8 (b) gives the relation between the real and imaginary capacitance with the frequency. The maximum capacitance is observed at lower frequency this is due to the capacitor acts as open circuits at lower frequency while it acts as a short circuit as the frequency goes to infinity. That is why the value of capacitance decreases with increasing frequency, as shown in Fig. 8 (b). In general, at low frequency SCs takes more time to charge and discharge, therefore all the active sites take part in charge storage. On the other hand, at higher frequency SCs takes very low time for charge-discharge process that results in lower capacitance.

Conclusion

The nanocomposites of rGO-PMo_{12} and rGO-PW_{12} were successfully synthesized by economical and scalable two-step process which led to the formation of homogeneously dispersed POMs nanoclusters on the rGO nanosheets. The prepared nano-hybrid led to reaching a maximum specific capacitance of 299 and 370 F/g for rGO-PMo_{12} and rGO-PW_{12}, respectively. The credit for this excellent electrochemical performance goes to unique architecture, better charge transport property of rGO and intimate contact of POMs nanoclusters with rGO. Moreover, the novel rGO-PMo_{12}//rGO-PW_{12} asymmetric cell is assembled which exhibits a specific capacitance of 110 F/g and 95 % cycling stability over 2000 cycles. In addition, the asymmetric cell shows high energy density of 39 Wh/kg and high power density of 6583 W/kg, suggesting the potential of this new hybrid device based on hybrid electrodes for many promising energy storage applications.

Acknowledgements

DPD acknowledges the support of University of Adelaide, Australia for grant of Research Fellowship (VC Fellow) and the Secretary for Universities and Research of the Ministry of Economy and Knowledge of the Government of Catalonia and the Co-fund programme of the Marie Curie Actions of the 7th R&D Framework Programme of the European Union".

References

[1] Dubal, D. P.; Ayyad, O.; Ruiz, V.; Gómez-Romero, P. Hybrid Energy Storage: The Merging of Battery and Supercapacitor Chemistries. *Chem. Soc. Rev.* **2015**, *44*, 1777–1790

[2] Simon, P.; Gogotsi, Y.; Dunn, B.; Where Do Batteries End and Supercapacitors Begin? *Science*, **2014**, 343,1210-1211

[3] Wang, G.; Zhang, L.; Zhang, J.; A review of electrode materials for electrochemical supercapacitors. *Chem. Soc. Rev.* **2012**, 41, 797-828

[4] Miller, J. R.; Simon, P.; Electrochemical capacitors for energy management. *Science* **2008**, 321, 651-652.

[5] Liu, L.; Niu, Z.; Chen, J.; Unconventional supercapacitors from nanocarbon-based electrode materials to device configurations, *Chem. Soc. Rev.*, **2016**, 45, 4340-4363

[6] Naoi, K.; Ishimoto. S.; Miyamoto, J. I.; Naoi, W.; Second generation 'nanohybrid supercapacitor': evolution of capacitive energy storage devices. *Energy Environ. Sci.* **2012**, 5, 9363-9373

[7] Zhang, F.; Zhang, T.; Yang, X.; Zhang, L.; Leng, K.; Huang, Y.; Chen, Y.; A high-performance supercapacitor-battery hybrid energy storage device based on graphene-enhanced electrode materials with ultrahigh energy density, *Energy Environ. Sci.*, **2013**, 6, 1623-1632

[8] Bose, S.; Kuila, T.; Mishra, A. K.; Rajasekar, R.; Kim, N. H.; Lee, J. H.; Carbon-based nanostructured materials and their composites as supercapacitor electrodes, *J. Mater. Chem.*, **2012**, 22, 767-784

[9] Dubal, D. P.; Holze, R.; Gomez-Romero, P.; Development of hybrid materials based on sponge supported reduced graphene oxide and transition metal hydroxides for

hybrid energy storage devices, *Sci. Rep.*, **2014**, 4, 7349

[10] Ji, Y.; Huang, L.; Hu, J.; Streb, C.; Song, Y. F.; Polyoxometalate-functionalized nanocarbon materials for energy conversion, energy storage and sensor systems, *Energy Environ. Sci.*, **2015**, 8, 776–789

[11] Cuentas-Gallegos, A.; Martinez-Rosales, R.; Baibarac, M.; Gomez-Romero, P.; Rincon, M. E.; Electrochemical Supercapacitors Based on Novel Hybrid Materials Made of Carbon Nanotubes and Polyoxometalates, *Electrochem. Commun.* **2007**, 9, 2088-2092.

[12] Ruiz, V.; Suarez-Guevara, J.; Gomez-Romero, P.; Hybrid Electrodes Based on Polyoxometalates-Carbon Materials for Electrochemical Supercapacitors. *Electrochem. Commun.*, **2012**, 24, 35-38.

[13] Suarez-Guevara, J.; Ruiz, V.; Gomez-Romero, P.; Hybrid Energy Storage: High Voltage Aqueous Supercapacitors Based on Activated Carbon-Phosphotungstate Hybrid Materials, *J. Mater. Chem. A*, **2014**, 2, 1014-1021

[14] Genovese, M.; Lian, K.; Polyoxometalate modified pine-cone biochar carbon for supercapacitor electrodes, *J. Mater. Chem. A*, **2017**, 5, 3939-3947

[15] Palomino, P.; Suarez-Guevara, J.; Olivares-Marin, M.; Ruiz, V.; Dubal, D. P.; Gomez-Romero, P.; Tonti, D.; Enciso, E.; Influence of texture in hybrid carbon-phosphomolybdic acid materials on their performance as electrodes in supercapacitors, *Carbon*, **2017**, 111, 74–82.

[16] Casan-Pastor, N.; Gomez-Romero, P.; Polyoxometalates: From Inorganic Chemistry to Materials Science, *Front. Biosci.* **2004**, 9, 1759-1770.

[17] Ammam, M.; Polyoxometalates: formation, structures, principal properties, main deposition methods and application in sensing, *J. Mater. Chem. A*, **2013**, 1, 6291–6312

[18] Dubal, D. P.; Ballesteros, B.; Mohite, A. A.; Gomez-Romero, P.; Functionalization of Polypyrrole Nanopipes with Redox-Active Polyoxometalates for High Energy Density Supercapacitors, *ChemSusChem* **2017**, 10, 731-737

[19] Genovese, M.; Lian, K.; Pseudocapacitive Behavior of Keggin Type Polyoxometalate Mixtures, *Electrochem. Commun.*, **2014**, 43, 60-62.

[20] Genovese, M.; Lian, K.; Polyoxometalate Modified Inorganic-Organic Nanocomposite Materials for Energy Storage Applications: A Review, *Curr. Opin. Solid State Mater. Sci.* **2015**, 19, 126-137

[21] Dubal, D. P.; Suarez-Guevara, J.; Tonti, D.; Enciso, E.; Gomez-Romero, P.; A high voltage solid state symmetric supercapacitor based on graphene–polyoxometalate hybrid electrodes with a hydroquinone doped hybrid gel-electrolyte, *J. Mater. Chem. A*, **2015**, 3, 23483–23492

[22] Suarez-Guevara, J.; Ruiz, V.; Gomez-Romero, P.; Stable graphene-polyoxometalate nanomaterials for application in hybrid supercapacitors, *Phys. Chem. Chem. Phys.*, 2014, 16, 20411–20414.

[23] Fleisch, T. H.; Mains, G. J.; An XPS study of the UV reduction and photochromism of MoO_3 and WO_3, *J. Chem. Phys.* **1982**, 76, 780

[24] Colton, R. J.; Guzman, A. M.; Rabalais, J. W.; Electrochromism in some thin-film transition-metal oxides characterized by x-ray electron spectroscopy, *J. Appl. Phys.* **1978**, 49, 409

[25] Wagner, C. D.; Riggs, W. M.; Davis, L. E.; Moulder, J. F. In Handbook of X-ray Photoelectron Spectroscopy; Muilenberg, G. E.; ed., Perkin Elmer Corp.: Eden Praire, MN, 1979, p. 146, and references therein.

[26] Yang, Y.; Ruan, G.; Xiang, C.; Wang, G.; Tour, J. M.; Flexible Three-Dimensional Nanoporous Metal-Based Energy Devices, *J. Am. Chem. Soc.* **2014**, *136*, 6187-6190.

[27] Hsu, C.T.; Hu, C.C.; Wu, T.H.; Chen, J.C.; Rajkumar, M.; How the electrochemical reversibility of a battery-type material affects the charge balance and performances of asymmetric supercapacitors, *Electrochim. Acta*, **2014**, 146, 759-768

[28] Suppes, G. M.; Cameron, C. G.; Freund, M. S.; A Polypyrrole/Phosphomolybdic Acid//Poly(3,4-ethylenedioxythiophene)/Phosphotungstic Acid Asymmetric Supercapacitor. *J. Electrochem. Soc.,* **2010**, 157**,** A1030-A1034

[29] Yuan, L. Y.; Lu, X. H.; Xiao, X.; Zhai, T.; Dai, J. J.; Zhang, F. C.; Hu, B.; Wang, X,; Gong, L.; Chen, J.; Hu, C.; Tong, Y.; Zhou, J.; Wang, Z. L.; Flexible solid-state supercapacitors based on carbon nanoparticles/MnO_2 nanorods hybrid structure. *ACS Nano* **2012**, 6, 656-661.

[30] Hsia, B.; Marschewski, J.; Wang, S.; In, J. B.; Carraro, C.; Poulikakos, D.; Grigoropoulos, C. P.; Maboudian, R.; Highly flexible, all solid-state micro-supercapacitors from vertically aligned carbon nanotubes. *Nanotechnology*, **2014**, 25, 055401.

[31] Aradilla, D.; Gaboriau, D.; Bidan, G.; Gentile, P.; Boniface, M.; Dubal, D. P.; Gomez-Romero, P.; Wimberg, J.; Schubert, T. S.J.; Sadki, S.; An innovative 3-D nanoforest heterostructure made of polypyrrole coated silicon nanotrees for new high performance hybrid micro-supercapacitors, *J. Mater. Chem. A*, **2015**, 3, 13978-13985

[32] Dubal, D. P.; Chodankar, N. R.; Holze, R.; Kim, D. H.; Gomez-Romero, P.; Ultrathin Mesoporous $RuCo_2O_4$ Nanoflakes: An Advanced Electrode for High-Performance Asymmetric Supercapacitors *ChemSusChem* **2017**, DOI: 10.1002/cssc.201700001

Figure captions

Fig. 1 (a, b) SEM images (c, d) STEM images of hybrid materials rGO-PMo_{12} and rGO-PW_{12} with corresponding TEM-EDS elemental analysis (e, f), respectively.

Fig. 2 (a) Full XPS spectra for rGO-PMo_{12} and rGO-PW_{12} hybrid materials, (b-d) high magnified XPS spectra for C1s, Mo3d and W4f, respectively.

Fig. 3 (a, b) cyclic voltammetry (CV) curves of rGO-PMo_{12} and rGO-PW_{12} hybrid electrodes at different scan rates, respectively, (c, d) galvanostatic charge/discharge (CD) curves of rGO-PMo_{12} and rGO-PW_{12} electrodes at different current densities, respectively, (e, f) Plots of specific and areal capacitances versus current density for rGO-PMo_{12} and rGO-PW_{12} hybrid electrodes, respectively

Fig. 4 (a) Plots of Log(anodic current density) versus Log(scan rate) for rGO-PMo_{12} and rGO-PW_{12} in order to determine the *b* -values in the CV curves from 5 to 100 mV/s in 1M H_2SO_4 electrolyte, (b) The plot of total gravimetric charge against the reciprocal of the square root of potential scan rate for rGO-PMo_{12} and rGO-PW_{12} hybrid electrodes, (c) The distribution of capacitive and diffusion controlled charge storage in rGO-PMo_{12} and rGO-PW_{12} hybrid electrdes at different scan rates

Fig. 5 Schematic illustration of fabrication of asymmetric supercapacitor with rGO-PMo_{12} as positive electrode and rGO-PW_{12} as negative electrode in order to achieve wide voltage window.

Fig. 6 (a) CV curves for rGO-PMo_{12}//rGO-PW_{12} asymmetric cell at different scan rates within operating voltage range from 0 to 1.6 V. (b) representative charge/discharge curve measured at

15 mA/cm^2 for the rGO-PMo_{12}//rGO-PW_{12} asymmetric cell with corresponding potential distribution across positive (rGO-PMo_{12}) and negative (rGO-PW_{12}) electrodes. (c) CD curves for rGO-PMo_{12}//rGO-PW_{12} cell at different current densities within 0 to 1.6 V and (d) variation of specific and volumetric capacitance at different current densities.

Fig. 7 (a) Ragone plot for rGO-PMo_{12}//rGO-PW_{12} asymmetric cell and (b) variation of Coulombic efficiency and capacitive retention with cycle numbers for rGO-PMo_{12}//rGO-PW_{12} device.

Fig. 8 (a) the Nyquist plot for rGO-PMo_{12}//rGO-PW_{12} asymmetric cell, inset shows bode plot and (b) the variation of real and imaginary capacitance with frequency for rGO-PMo_{12}//rGO-PW_{12} device.

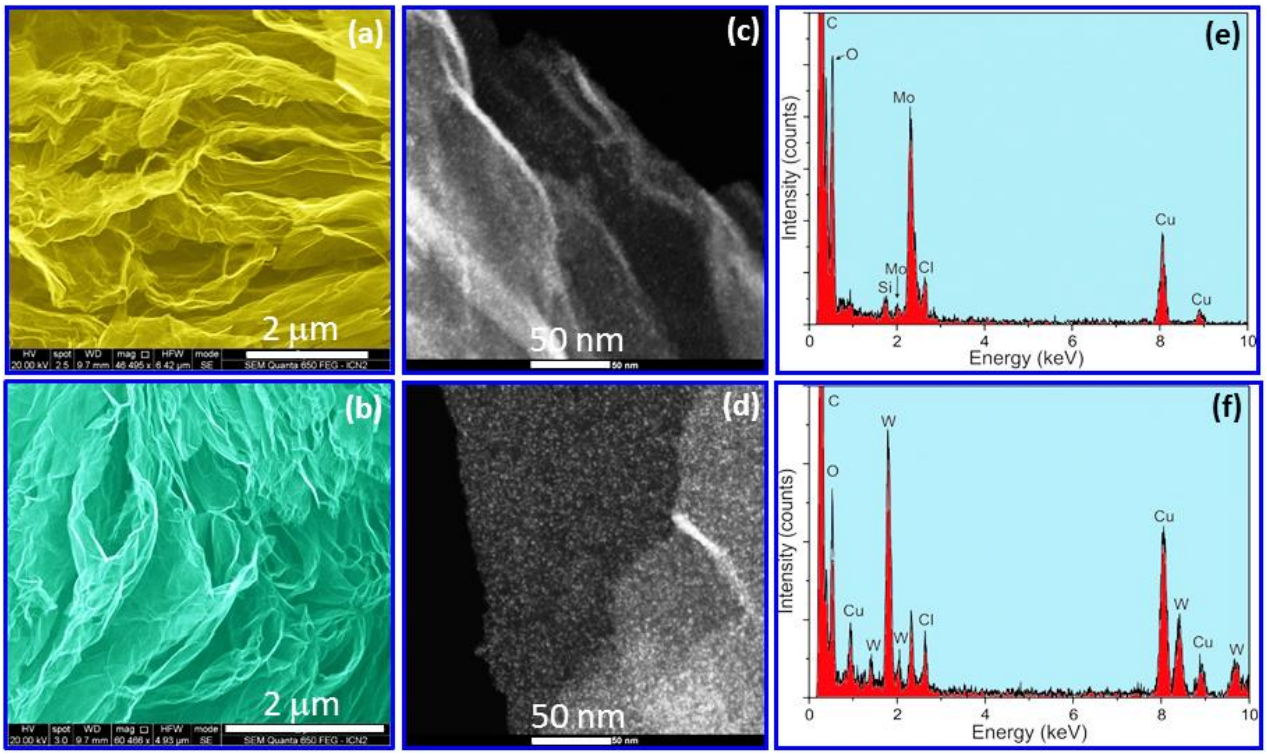
(a)
2 µm
(c)
50 nm
(e)
C
O
Mo
Cu
Mo
Si
Cl
Cu
Intensity (counts)
0
2
4
6
8
10
Energy (keV)
(b)
2 µm
(d)
50 nm
(f)
C
W
O
Cu
Cu
W
W
Cl
W
Cu
W
Intensity (counts)
0
2
4
6
8
10
Energy (keV)

Fig. 1

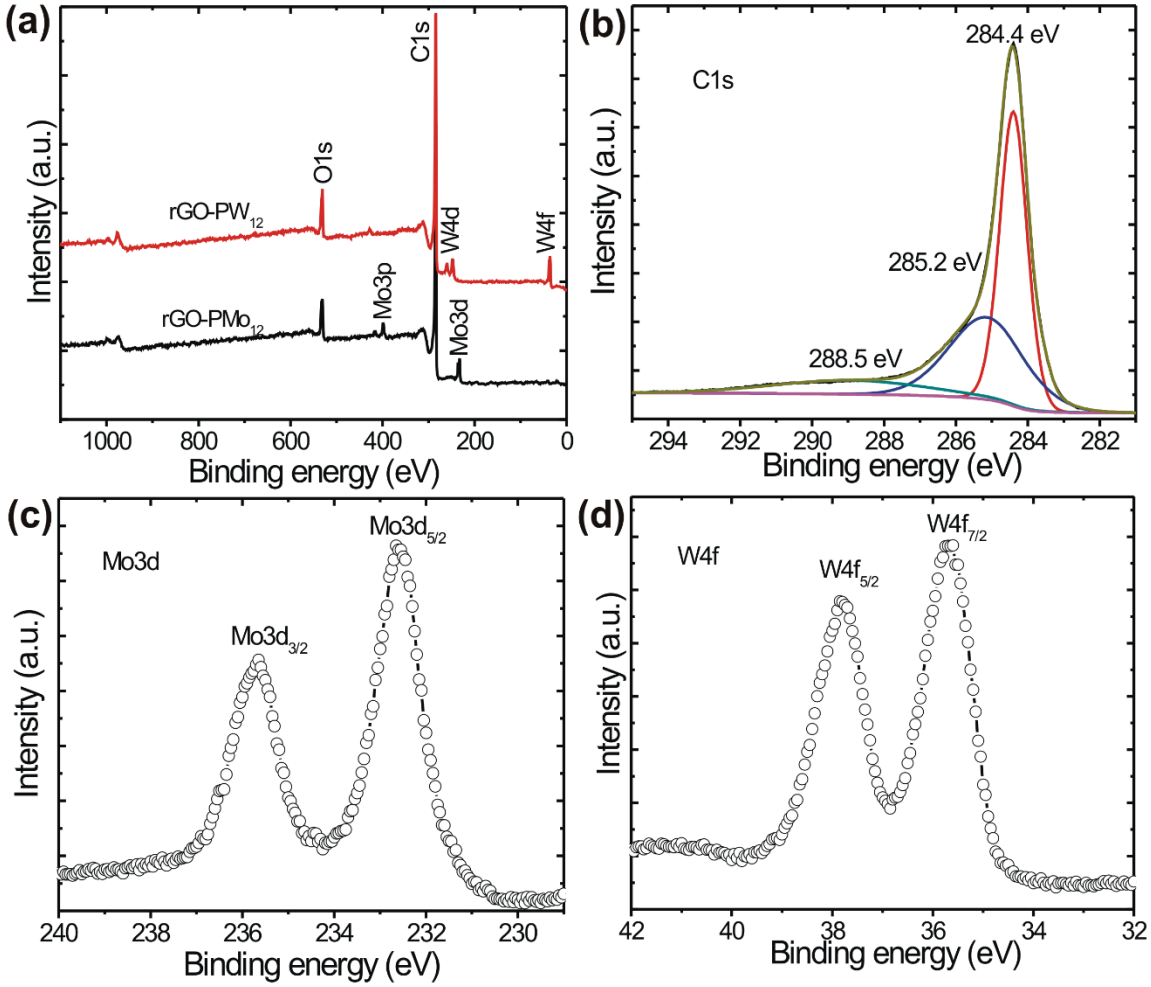
(a)
Intensity (a.u.)
C1s
O1s
W4d
W4f
Mo3p
Mo3d
rGO-PW12
rGO-PMo12
1000
800
600
400
200
0
Binding energy (eV)
(b)
C1s
284.4 eV
285.2 eV
288.5 eV
Intensity (a.u.)
294
292
290
288
286
284
282
Binding energy (eV)
(c)
Mo3d
Mo3d5/2
Mo3d3/2
Intensity (a.u.)
240
238
236
234
232
230
Binding energy (eV)
(d)
W4f
W4f7/2
W4f5/2
Intensity (a.u.)
42
40
38
36
34
32
Binding energy (eV)

Fig. 2

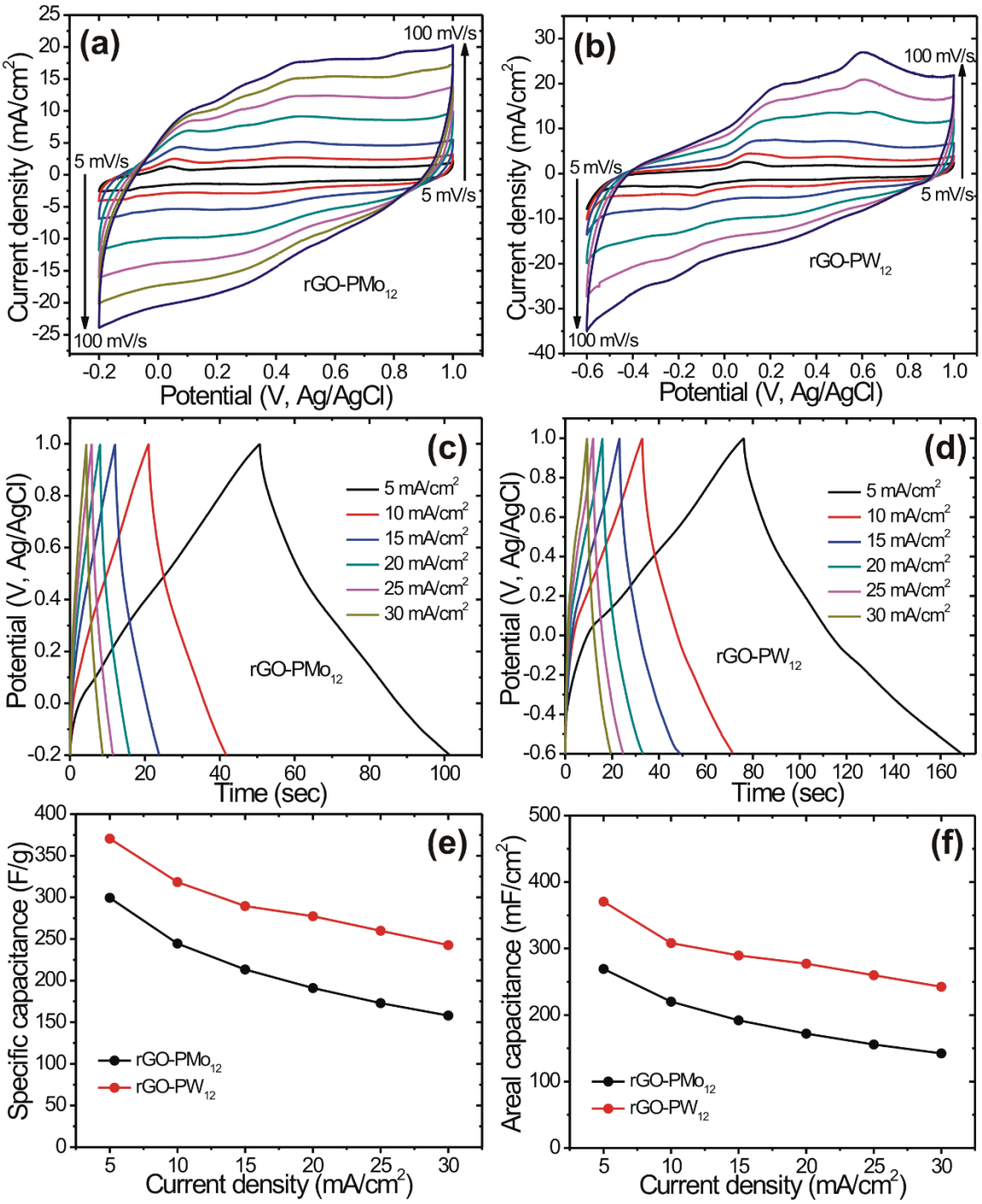
(a)
100 mV/s
5 mV/s
5 mV/s
100 mV/s
rGO-PMo12
Current density (mA/cm2)
Potential (V, Ag/AgCl)
(b)
100 mV/s
5 mV/s
5 mV/s
100 mV/s
rGO-PW12
Current density (mA/cm2)
Potential (V, Ag/AgCl)
(c)
5 mA/cm2
10 mA/cm2
15 mA/cm2
20 mA/cm2
25 mA/cm2
30 mA/cm2
rGO-PMo12
Potential (V, Ag/AgCl)
Time (sec)
(d)
5 mA/cm2
10 mA/cm2
15 mA/cm2
20 mA/cm2
25 mA/cm2
30 mA/cm2
rGO-PW12
Potential (V, Ag/AgCl)
Time (sec)
(e)
rGO-PMo12
rGO-PW12
Specific capacitance (F/g)
Current density (mA/cm2)
(f)
rGO-PMo12
rGO-PW12
Areal capacitance (mF/cm2)
Current density (mA/cm2)

Fig. 3

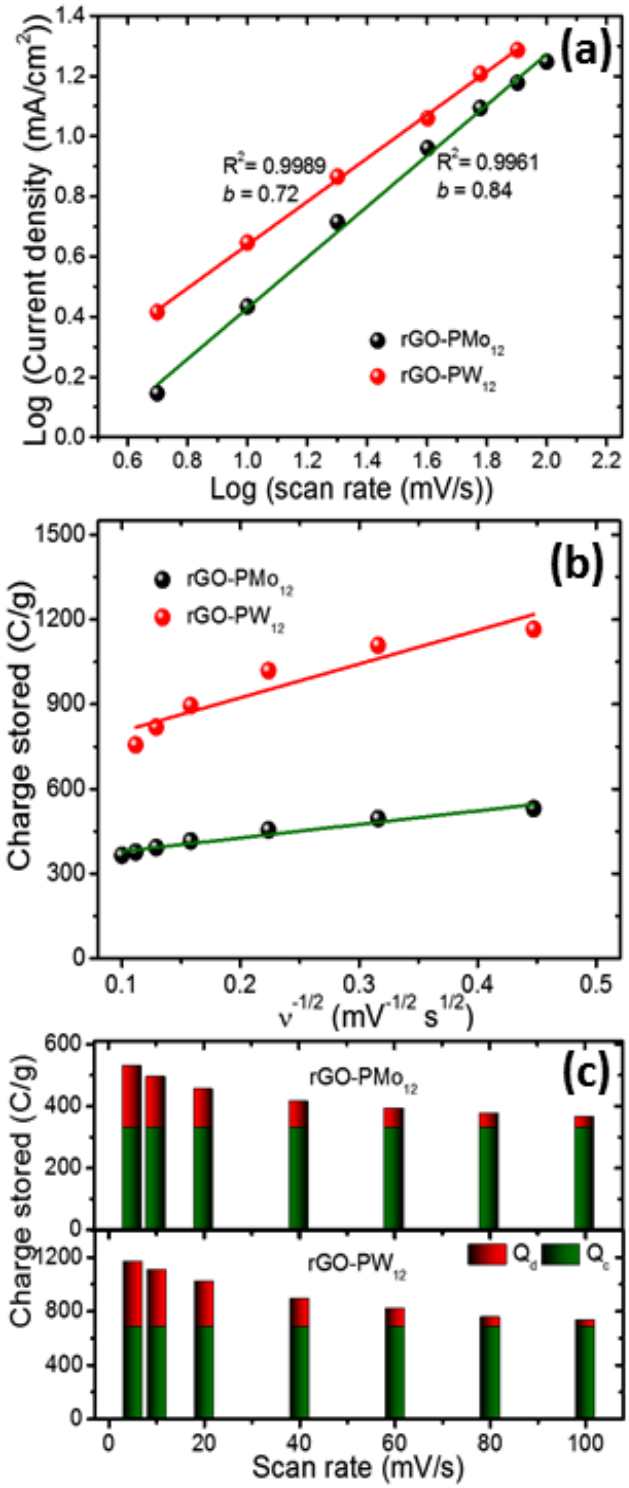
(a)
Log (Current density (mA/cm^2))
Log (scan rate (mV/s))
R^2= 0.9989
b = 0.72
R^2= 0.9961
b = 0.84
rGO-PMo$_{12}$
rGO-PW$_{12}$
(b)
Charge stored (C/g)
$\nu^{-1/2}$ (mV$^{-1/2}$ s$^{1/2}$)
(c)
Charge stored (C/g)
Scan rate (mV/s)
Q_d
Q_c

Fig. 4

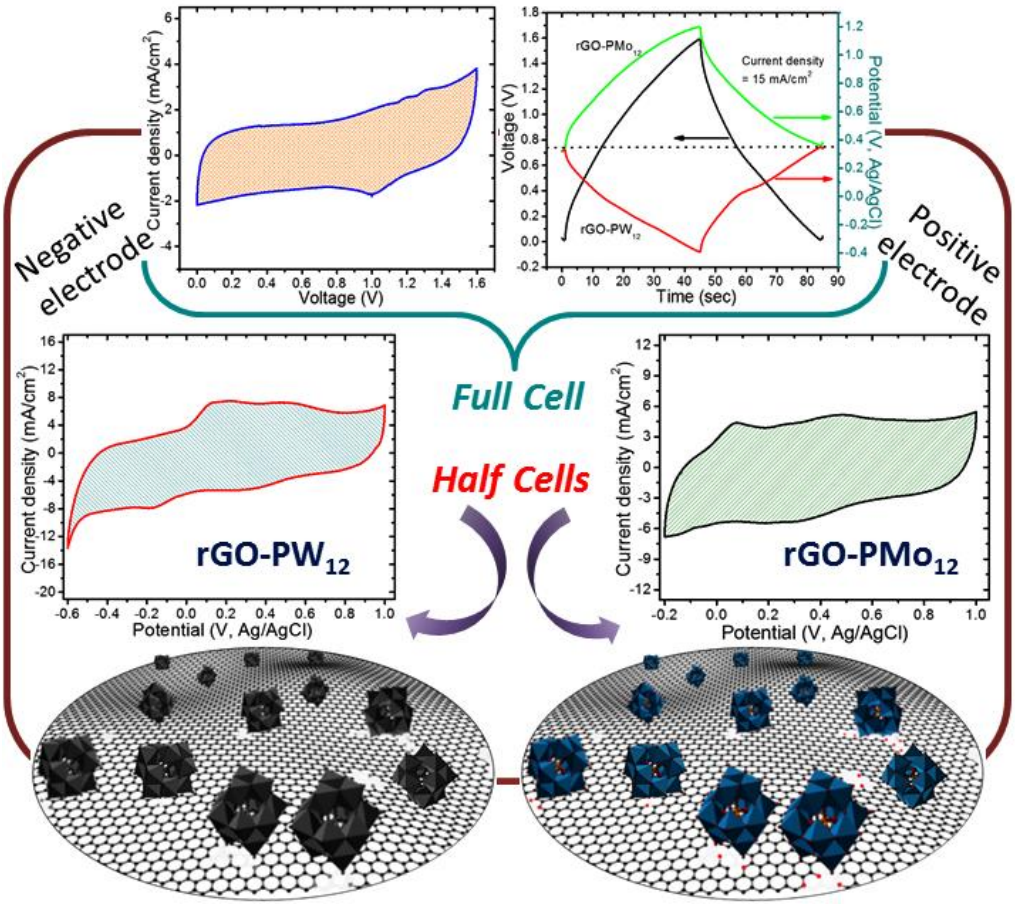
Negative electrode
Positive electrode
Current density (mA/cm²)
Voltage (V)
rGO-PMo12
rGO-PW12
Current density = 15 mA/cm²
Voltage (V)
Potential (V, Ag/AgCl)
Time (sec)
Full Cell
Half Cells
rGO-PW12
rGO-PMo12
Current density (mA/cm²)
Potential (V, Ag/AgCl)

Fig. 5

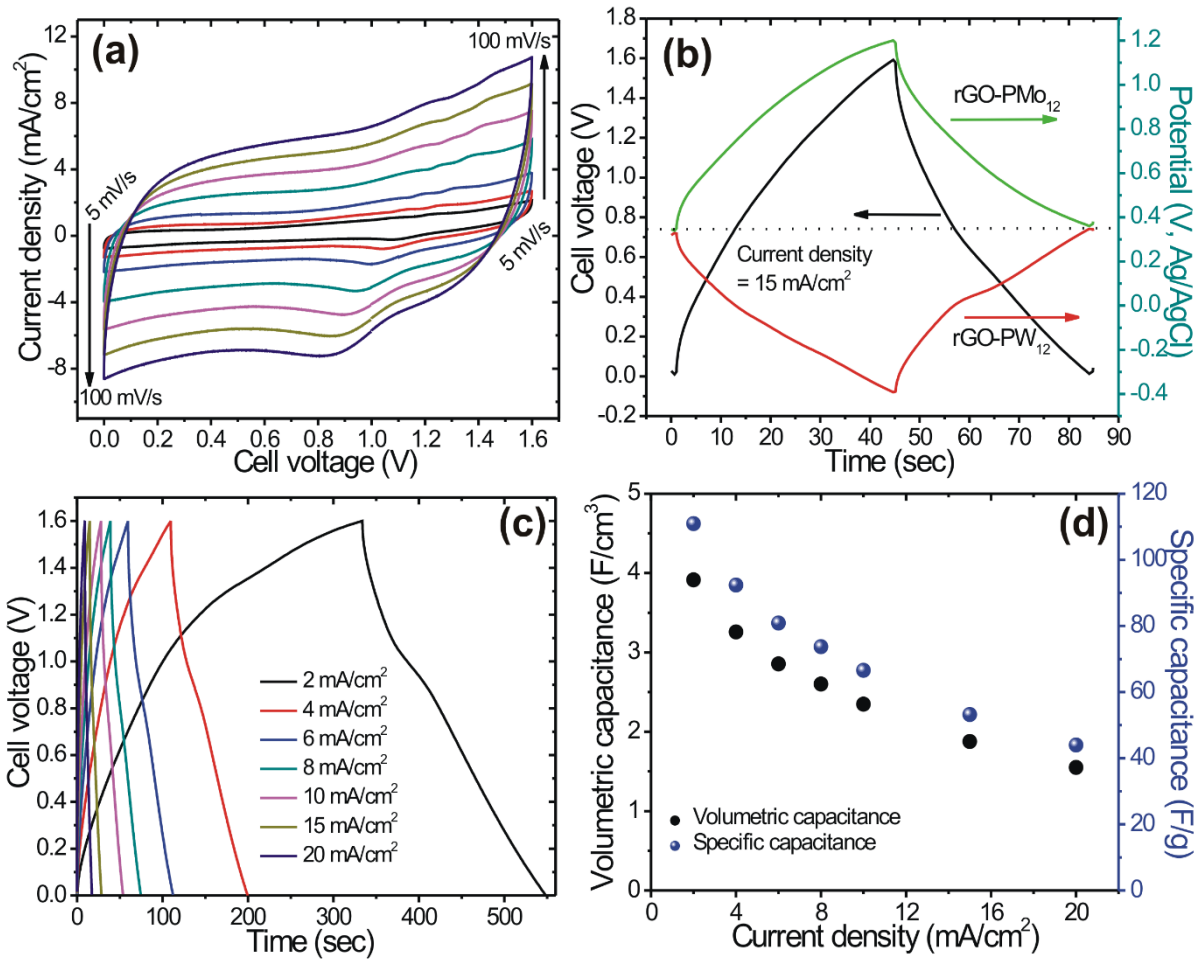
(a)
100 mV/s
5 mV/s
5 mV/s
100 mV/s
Current density (mA/cm²)
Cell voltage (V)
(b)
rGO-PMo12
Current density
= 15 mA/cm²
rGO-PW12
Cell voltage (V)
Potential (V, Ag/AgCl)
Time (sec)
(c)
2 mA/cm²
4 mA/cm²
6 mA/cm²
8 mA/cm²
10 mA/cm²
15 mA/cm²
20 mA/cm²
Cell voltage (V)
Time (sec)
(d)
Volumetric capacitance
Specific capacitance
Volumetric capacitance (F/cm³)
Specific capacitance (F/g)
Current density (mA/cm²)

Fig. 6

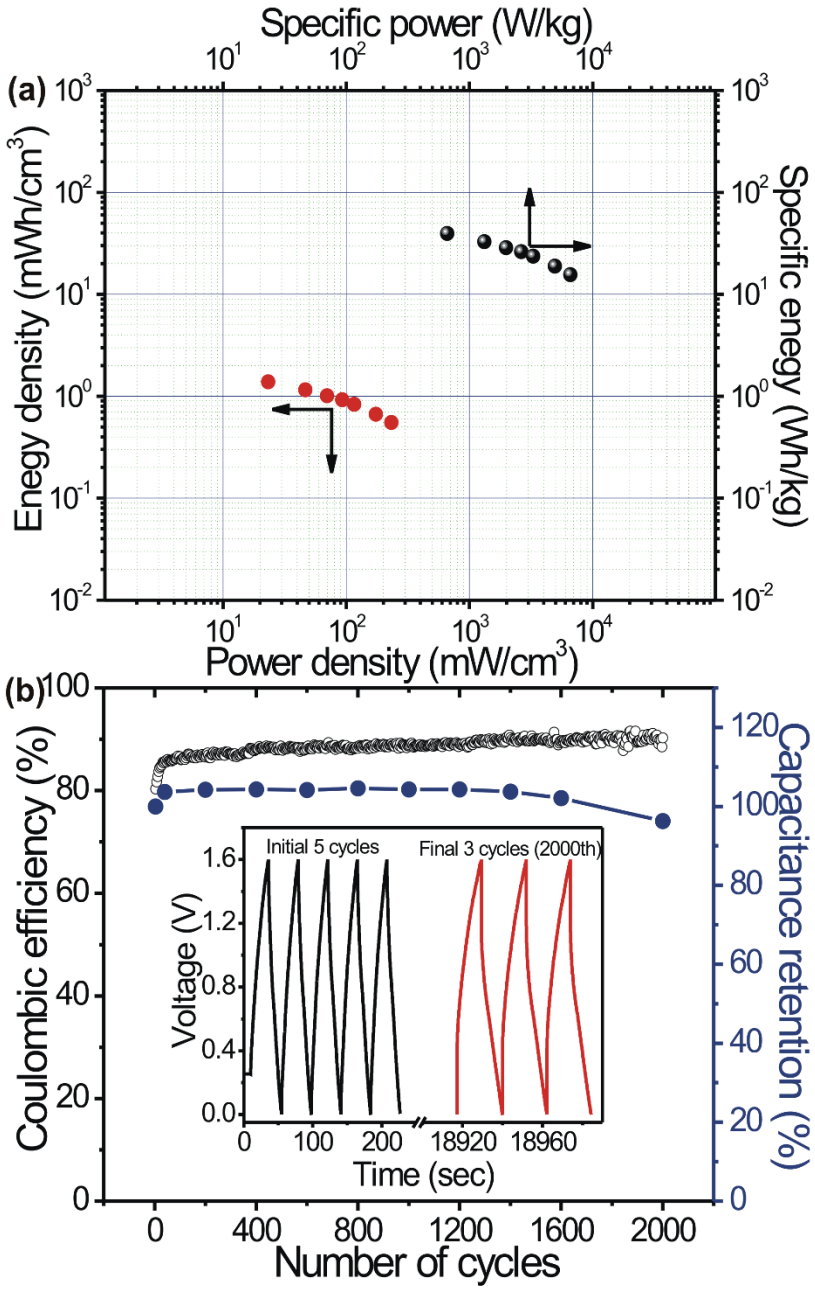
(a)
Specific power (W/kg)
Enegy density (mWh/cm3)
Specific enegy (Wh/kg)
Power density (mW/cm3)
(b)
Coulombic efficiency (%)
Capacitance retention (%)
Number of cycles
Initial 5 cycles
Final 3 cycles (2000th)
Voltage (V)
Time (sec)

Fig. 7

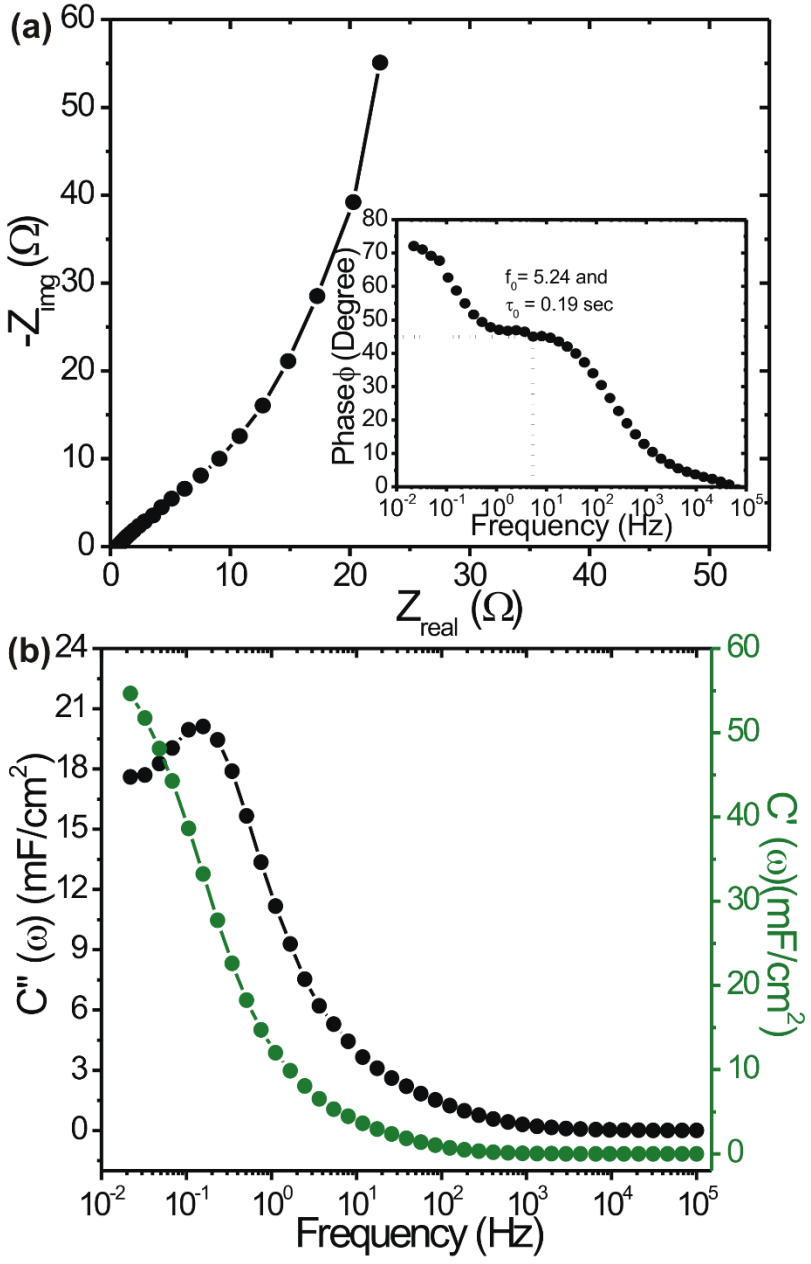
(a)
-Z_img (Ω)
Z_real (Ω)
Phase ϕ (Degree)
f_0 = 5.24 and
τ_0 = 0.19 sec
Frequency (Hz)
(b)
C'' (ω) (mF/cm²)
C' (ω)(mF/cm²)
Frequency (Hz)

Fig. 8